Diagonal Elements

Differentiate Eq. (A6) to obtain

$$g''(\tau) = [(\beta-\alpha)-(\alpha+\beta)\tau]P_N^{\prime\prime(\alpha,\beta)} + [N(N+\alpha+\beta+1) - (\alpha+\beta)]P_N^{\prime(\alpha,\beta)} \tag{B3}$$

At the internal nodes τ_j, $1 \le j \le N-1$, $P_N^{\prime(\alpha,\beta)} = 0$ by definition of the nodes. Utilizing Eq. (A4), one obtains

$$P_N^{\prime\prime(\alpha,\beta)}(\tau_j) = \frac{N(N+\alpha+\beta+1)P_N^{(\alpha,\beta)}(\tau_j)}{\left(\tau_j^2-1\right)} \tag{B4}$$

Substituting Eqs. (A7), (B3), and (B4) into Eq. (B2) yields

$$\phi_j'(\tau_j) = \frac{(\alpha+\beta)\tau_j + \alpha - \beta}{2\left(1-\tau_j^2\right)}, \qquad j = 1, \ldots, N-1 \tag{B5}$$

For the endpoint expressions, differentiate Eq. (A4) to obtain

$$P_N^{\prime\prime(\alpha,\beta)}(\tau_0) = \frac{[N(N+\alpha+\beta+1)-(\alpha+\beta+2)]}{2(\beta+2)} \times \frac{N(N+\alpha+\beta+1)P_N^{(\alpha,\beta)}(\tau_0)}{2(\beta+1)} \tag{B6}$$

$$P_N^{\prime\prime(\alpha,\beta)}(\tau_N) = \frac{[N(N+\alpha+\beta+1)-(\alpha+\beta+2)]}{2(\alpha+2)} \times \frac{N(N+\alpha+\beta+1)P_N^{(\alpha,\beta)}(\tau_N)}{2(\alpha+1)} \tag{B7}$$

Substituting Eqs. (B6) and (B7), together with Eqs. (A8) and (A9), into Eq. (B3) gives expressions for $g''(\tau_0)$ and $g''(\tau_N)$, which may be substituted into Eq. (B2) to give the remaining matrix elements.

References

[1]Betts, J. T., "Survey of Numerical Methods for Trajectory Optimization," *Journal of Guidance, Control, and Dynamics*, Vol. 21, No. 2, 1998, pp. 193–207.

[2]Herman, A. L., and Conway, B. A., "Direct Optimization Using Collocation Based on High-Order Gauss–Lobatto Quadrature Rules," *Journal of Guidance, Control, and Dynamics*, Vol. 19, No. 3, 1996, pp. 592–599.

[3]Enright, P. J., and Conway, B. A., "Discrete Approximations to Optimal Trajectories Using Direct Transcription and Nonlinear Programming," *Journal of Guidance, Control, and Dynamics*, Vol. 15, No. 4, 1992, pp. 994–1002.

[4]Hargraves, C. R., and Paris, S. W., "Direct Trajectory Optimization Using Nonlinear Programming and Collocation," *Journal of Guidance, Dynamics, and Control*, Vol. 10, No. 4, 1987, pp. 338–342.

[5]Elnagar, G., Kazemi, M. A., and Razzaghi, M., "The Pseudospectral Legendre Method for Discretizing Optimal Control Problems," *IEEE Transactions on Automatic Control*, Vol. 40, No. 10, 1995, pp. 1793–1796.

[6]Fahroo, F., and Ross, I. M., "Costate Estimation by a Legendre Pseudospectral Method," *Journal of Guidance, Control, and Dynamics*, Vol. 24, No. 2, 2001, pp. 270–277.

[7]Elnagar, G. M., and Kazemi, M. A., "Pseudospectral Chebyshev Optimal Control of Constrained Nonlinear Dynamical Systems," *Computational Optimization and Applications*, Vol. 11, No. 2, 1998, pp. 195–217.

[8]Fahroo, F., and Ross, I. M., "Direct Trajectory Optimization by a Chebyshev Pseudospectral Method," *Journal of Guidance, Control, and Dynamics*, Vol. 25, No. 1, 2002, pp. 160–166.

[9]Dontchev, A. L., Hager, W. W., and Veliov, V. M., "Second-Order Runge–Kutta Approximations in Control Constrained Optimal Control," *SIAM Journal of Numerical Analysis*, Vol. 38, No. 1, 2000, pp. 202–226.

[10]Ross, I. M., and Fahroo, F., "A Perspective on Methods for Trajectory Optimization," AIAA Paper 2002-4727, Aug. 2002.

[11]Fornberg, B., and Sloan, D. M., "A Review of Pseudospectral Methods for Solving Partial Differential Equations," *Acta Numerica*, Vol. 3, Aug. 1994, pp. 203–267.

[12]Gautschi, W., "High-Order Gauss–Lobatto Formulae," *Numerical Algorithms*, Vol. 25, No. 1, 2000, pp. 213–222.

[13]Ross, I. M., Rea, J., and Fahroo, F., "Exploiting Higher-Order Derivatives in Computational Optimal Control," *Proceedings of the MED 2002*, Mediterranean Conference on Control and Automation, Lisbon, Portugal, July 2002.

[14]Trefethen, L. N., *Spectral Methods in MATLAB*, SIAM Press, Philadelphia, 2000, pp. 124, 125.

[15]Gill, P. E., Murray, W., Saunders, M. A., and Wright, M. A., "User's Guide to NPSOL 5.0: A Fortran Package for Nonlinear Programming," Stanford Optimization Lab., Rept. TR SOL 86-1, Stanford Univ., Stanford, CA, July 1998.

[16]Bryson, A. E., *Dynamic Optimization*, Addison–Wesley, New York, 1999, Chap. 3.

Interferometric Observatories in Earth Orbit

I. I. Hussein,* D. J. Scheeres,† and D. C. Hyland‡
University of Michigan,
Ann Arbor, Michigan 48109-2140

I. Introduction

WE propose a class of satellite constellations that can act as interferometric observatories in Earth orbit. Based on techniques discussed in Refs. 1–3, the satellite constellation is capable of forming high-resolution images in timescales of a few hours without the need for active control beyond that needed for corrective maneuvers. First, we discuss the requirements to achieve these imaging goals. Next, we define a class of constellations that can achieve these goals. An optimization procedure is also defined that supplies m pixels of resolution with a minimum number of satellites. For the example considered, this procedure results in an observatory that is within 0–2 satellites from a lower bound of $\sqrt{m}$ satellites. The zonal J_2 effect is used to scan the observatory across the celestial sphere. Finally, we discuss the practical implementation of these observatories.

II. Imaging Requirements

Interferometric imaging is performed by measuring the mutual intensity (the two-point correlation[4]) that results from the collection and subsequent interference of two electric field measurements of a target made at two different observation points. While moving relative to each other, the satellites collect and transmit these measurements, which are later combined at a central node by use of precise knowledge of their locations and timing of data collection. A least-squares-error estimate of the image can be reconstructed given the mutual intensity measurements, parameters of the optical system, and the physical configuration of the observatory. To assess the quality of the reconstructed image, the reconstructed image is Fourier transformed into a two-dimensional plane of spatial frequencies (the wave number plane). At any given point on the wave number plane, the modulation transfer function (MTF) is defined as the ratio of the estimated intensity to the true image intensity. For an interferometric imaging constellation, the MTF can be

Received 4 April 2003; revision received 2 October 2003; accepted for publication 3 October 2003.

*Ph.D. Candidate, Department of Aerospace Engineering; ihussein@umich.edu. Member AIAA.

†Associate Professor, Department of Aerospace Engineering; scheeres@umich.edu. Associate Fellow AIAA.

‡Professor and Chair, Department of Aerospace Engineering; dhiland@engin.umich.edu.

computed given the measurement history and corresponding relative position data among the light-collecting spacecraft. In the wave number plane, a point with a zero MTF value implies that the system is "blind" to the corresponding sinusoidal pattern, whereas a large value of the MTF implies that the image signal can be restored at that wave number via an inverse Fourier transform (see Refs. 1–3). The MTF, as a measure of the imaging system's performance, is a function of both the optical system and the configuration of the observatory in physical space. In this Note we address the issue of designing the configuration of an interferometric observatory that ensures a nonzero value of the MTF within a desired region in the wave number plane.

For a general satellite constellation, denote the position vector of satellites i and j by $\boldsymbol{R}_i$ and $\boldsymbol{R}_j$, respectively, $i, j = 0, 1, \ldots, N-1$, where N is the number of satellites. Let $\boldsymbol{R}_{ij} = \boldsymbol{R}_j - \boldsymbol{R}_i$ be the relative position vector between satellites i and j and $\boldsymbol{r}_{ij}$ be the projection of $\boldsymbol{R}_{ij}$ onto a plane perpendicular to the line of sight of the observatory. Let $\bar{z}$ be the distance from the image plane to the observation plane. Denote by the term picture frame the angular extent of the intended image on the image plane. The picture frame is user defined and has a diameter of length $\bar{L}$. When the image plane is pixelated into an $m \times m$ grid, the size of each pixel is $L = \bar{L}/m$, and the resulting angular resolution is $\theta_r = L/\bar{z}$. Additionally, the angular extent of the desired picture frame is given by $\theta_p = \bar{L}/\bar{z}$, which leads to $\theta_p = m\theta_r$. Moreover, we assume that θ_p is much smaller than the field-of-view angular extent of the spacecraft apertures.

Dimensions of features in the wave number plane are the reciprocals of the corresponding dimensions in the physical plane. Thus, the resolution disk is a disk of diameter $1/\theta_r$ and is the region where we desire the MTF to have nonzero values (henceforth, simply denoted by wave number plane coverage). The picture frame region is a circular disk of diameter $1/\theta_p$. Therefore, the diameter of the resolution disk is m times the diameter of the picture frame disk in the wave number plane (Fig. 1). As the relative position vector of two spacecraft varies in the physical plane, the picture frame disk moves in the wave number plane, where its center follows the trajectory of the vector given by $\pm\boldsymbol{r}_{ij}/\lambda$, where λ is the imaging wavelength of interest. Each satellite, by itself, will contribute a disk that is centered at the origin with a diameter of $1/\theta_p$, and each pair of satellites will contribute two disks of diameter $1/\theta_p$ located 180 deg apart with a radius of r_{ij}/λ from the center, where $r_{ij} = |\boldsymbol{r}_{ij}|$. Define the minimum relative distance between satellites to be $d_{\min} = \lambda/\theta_p$. To cover completely the resolution disk in the wave number plane, it is sufficient to have satellites distributed such that there exist pairs with relative distances $d_{\min}, 2d_{\min}, \ldots, \frac{1}{2}(m-1)d_{\min}$. Let $d_{\max} = \frac{1}{2}(m-1)d_{\min}$.

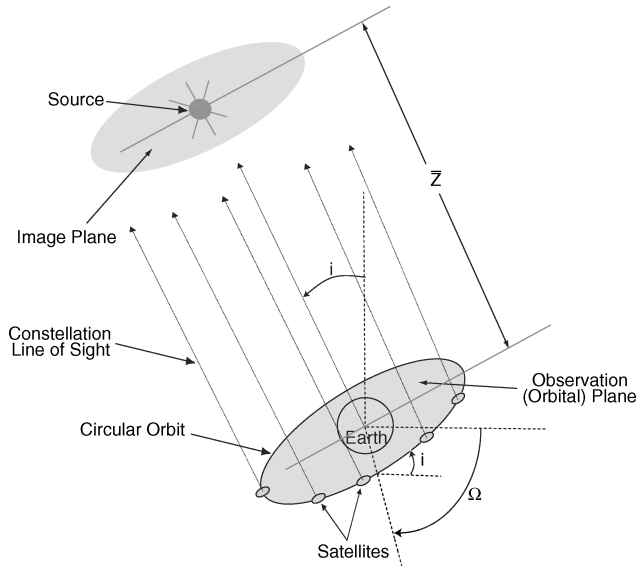

Fig. 1a Three-dimensional view of imaging observatory (not to scale).

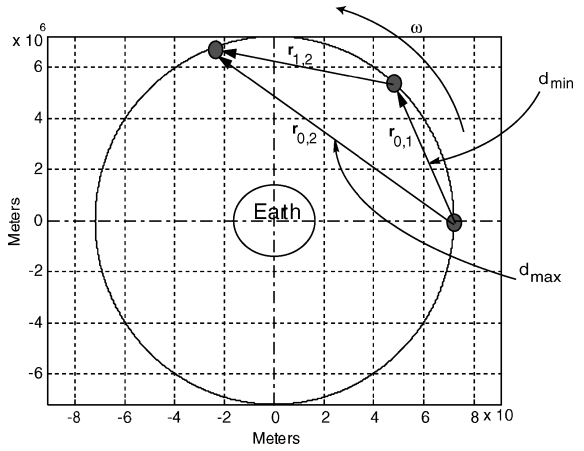

Fig. 1b Physical distribution in the orbit for $N_f = 3$ (not to scale).

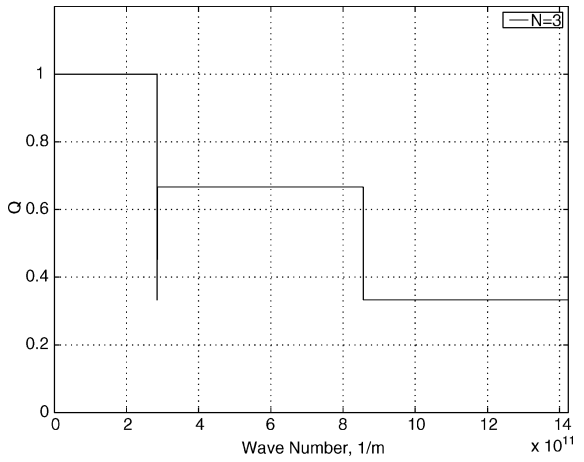

Fig. 1c Q curve for $N_f = 3$ in the fundamental constellation.

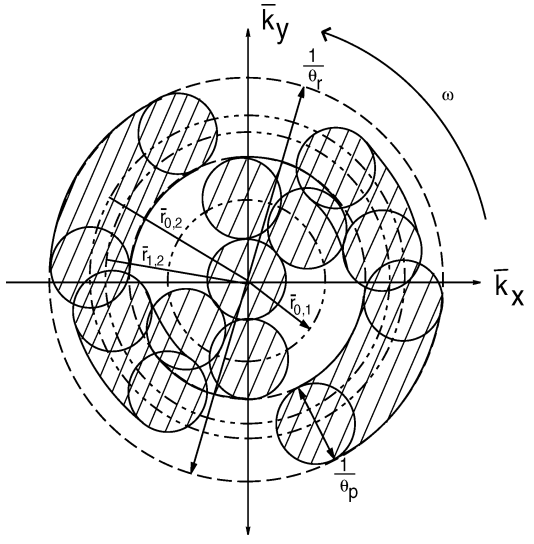

Fig. 1d Physical distribution in the wave number plane for $N_f = 3$, $m = 5$ (not to scale).

III. Circular Orbit Constellations

We propose a class of very long baseline constellations that achieve the requirement that the wave number plane be completely covered. The observatory design we propose here is a natural extension of very long baseline interferometric (VLBIs) linear, Earth-based observatories[5] to space-based, curved array VLBIs. The satellite constellation is placed on a circular arc that is a segment of an Earth orbit and whose center is located at the center of the Earth

(Fig. 1). The satellites are distributed such that the second satellite is located at a distance of $d_{\min}$ from the first satellite, the third at $2d_{\min}$ from the first, the fourth at $3d_{\min}$ from the first, and so on. Thus, a constellation of N_f satellites will have the Nth satellite located at a distance of $d_{\max} = (N-1)d_{\min}$. This distribution, defined as the "fundamental" constellation, implies that there are $m = 2N_f - 1$ pixels and ensures the complete coverage of the wave number plane, once the constellation is rotated 180 deg, that is, after half an orbit period. Figure 1 shows the geometry of this configuration for $N_f = 3$ satellites ($m = 5$ pixels). We nominally assume that the orbit plane is perpendicular to the line of sight to the target.

To compute the precise locations of the satellites in the constellation, we must specify the wavelength of interest, λ, and the desired angular extent of the picture frame $\theta_p = \bar{L}/\bar{z}$, which is sufficient to specify $d_{\min} = \lambda/\theta_p$. Given a number of satellites N_f, or the number of pixels m, one then obtains the corresponding angular resolution θ_r. The results presented in this Note are valid for all wavelengths and picture frame sizes such that $d_{\min}/r_o = 0.0791$ is a low-Earth-orbit radius, where $r_o = 7200$ km. This choice for $d_{\min}/r_o$ corresponds to an entire range of applications from $\lambda = 10$ μm, that is, an infrared (IR) interferometer, with a picture frame of angular extent equal to $\theta_p = 1.756 \times 10^{-10}$ to a value of $\lambda = 10$ m, that is, a radio interferometer, with a picture frame of angular extent equal to $\theta_p = 1.756 \times 10^{-5}$.

Let $\hat{\boldsymbol{\imath}}$ and $\hat{\boldsymbol{\jmath}}$ be two orthogonal unit vectors in the orbit plane; the position vector of the kth satellite, $k = 0, \ldots, N_f - 1$, is

$$\begin{aligned}\boldsymbol{r}_k(t) = r_o\Big(\Big\{&\cos(\omega t)\Big[1 - (k^2/2)(d_{\min}/r_o)^2\Big] \\ &- \sin(\omega t)k(d_{\min}/r_o)\sqrt{1-(k/2)^2(d_{\min}/r_o)^2}\Big\}\hat{\boldsymbol{\imath}} \\ &+\Big\{\sin(\omega t)\Big[1-(k^2/2)(d_{\min}/r_o)^2\Big] \\ &+\cos(\omega t)k(d_{\min}/r_o)\sqrt{1-(k/2)^2(d_{\min}/r_o)^2}\Big\}\hat{\boldsymbol{\jmath}}\Big)\end{aligned} \tag{1}$$

where ω is the orbit angular velocity of the nominal circular orbit

$$\omega = \sqrt{\mu/r_o^3} \tag{2}$$

and r_o is the orbit radius. The relative position vector from satellite l to satellite k is given by

$$\begin{aligned}\boldsymbol{r}_{lk}(t) = d_{\min}\Big(\Big\{&\cos(\omega t)(l^2-k^2)(d_{\min}/2r_o) \\ &+\sin(\omega t)\Big[-k\sqrt{1-k^2(d_{\min}/2r_o)^2}+l\sqrt{1-l^2(d_{\min}/2r_o)^2}\Big]\Big\}\hat{\boldsymbol{\imath}} \\ &+\Big\{\sin(\omega t)(l^2-k^2)(d_{\min}/2r_o) \\ &+\cos(\omega t)\Big[k\sqrt{1-k^2(d_{\min}/2r_o)^2}-l\sqrt{1-l^2(d_{\min}/2r_o)^2}\Big]\Big\}\hat{\boldsymbol{\jmath}}\Big)\end{aligned} \tag{3}$$

In the wave number plane, the relative position vector is $\bar{\boldsymbol{r}}_{lk} = \boldsymbol{r}_{lk}/\lambda$, a vector emanating from the origin with its tip at the center of the picture frame disk. When orbit perturbations are ignored, the preceding satellite arrangement guarantees that each $\bar{\boldsymbol{r}}_{lk}$ has a constant magnitude (because they are distributed along the same circular orbit), which is given by

$$\bar{r}_{lk} = (2r_o\sigma/\lambda)\sqrt{[(\hat{l}^2-\hat{k}^2)\sigma]^2 + \Big[\hat{k}\sqrt{1-(\hat{k}\sigma)^2} - \hat{l}\sqrt{1-(\hat{l}\sigma)^2}\Big]^2} \tag{4}$$

where $\hat{l} = l/(N_f - 1)$, $\hat{k} = k/(N_f - 1)$, $l, k = 0, 1, 2, \ldots, N_f - 1$, and $\sigma = d_{\max}/2r_o$. Note that $0 < \sigma \leq 1$, where $\sigma \to 0$ as either $d_{\max} \to 0$ or $r_o \to \infty$. The latter case arises if the constellation is placed on an orbit with small curvature. As $\sigma \to 0$, we have $\bar{r}_{lk} \to d_{\min}|k-l|/\lambda$. Note that $\sigma = 1$ only when $d_{\max} = 2r_o$, that is, when the constellation spans 180 deg. On the other hand, note that for all N_f we have $0 \leq \hat{l}, \hat{k} \leq 1$ and that variations in N_f do not induce variations on $\bar{r}_{lk}$.

Note that all $\bar{\boldsymbol{r}}_{lk}$ rotate at the same (constant) rate ω and that this constellation will sweep out the resolution disk in the wave number plane over half an orbit. If the line of sight is tilted away from the orbit normal by an angle ϵ, coverage of the wave number plane will range from full resolution θ_r to a maximum resolution of $\theta_r/\cos\epsilon$. Figure 1 shows the wave number plane coverage for $N_f = 3$. Note that imaging in the opposite direction is possible by rotating the spacecraft 180 deg about the radius vector.

IV. Minimizing Number of Satellites for a Given Resolution

In the fundamental constellation, we define the fundamental baselines by $\bar{\boldsymbol{r}}_{0,k}$ and the bonus baselines by $\bar{\boldsymbol{r}}_{l,k}$, $l \neq 0$. By themselves, the fundamental baselines guarantee complete coverage of the wave number plane over half an orbit period, and the bonus baselines provide redundant coverage. For large N_f, there will be an excessive number of multiple coverage areas, which implies that the number of satellites can be reduced with the resolution disk still being completely covered.

To carry out this minimization, it is not necessary to consider the two-dimensional wave number plane and is sufficient to consider the one-dimensional wave number space. Define a ray in the wave number plane parameterized by the radius $\bar{k}_r \in [0, \bar{k}_{\max}]$, where $\bar{k}_{\max} = 1/(2\theta_r)$. Let the contribution of each pair of satellites (l, k) to the image coverage be given by

$$f_{lk}(\bar{k}_r) = \begin{cases} 1 & \text{if} \quad \bar{k}_r \in [\bar{r}_{lk} - (\bar{d}_{\min}/2), \bar{r}_{lk} + (\bar{d}_{\min}/2)] \\ 0 & \text{otherwise} \end{cases} \tag{5}$$

for $l = 0, \ldots, N-1$ and $k = l, \ldots, N-1$. Next, define the function

$$Q(\bar{k}_r) = \frac{1}{N}\sum_{l=0}^{N-1}\sum_{k=l}^{N-1} f_{lk}(\bar{k}_r)$$

which is the superposition of all contributions. Figure 1 shows Q for $N = N_f = 3$ ($m = 5$ pixels) and Fig. 2 shows Q for $N_f = 16$ ($m = 31$). For the $N_f = 1, 2, 3$, and 4 cases, removing any satellite will immediately cause a portion of the resolution disk to not be covered; thus, the minimum number of satellites for these cases is $N_{\min}(m) = \frac{1}{2}(m+1)$. For larger numbers of satellites, that is, larger number of pixels, m, this is not true.

Our current minimization problem is stated as follows: Start from a fundamental constellation, with a corresponding fixed number of pixels m, and maximize the number of satellites that can be removed from the constellation under the constraint that $Q(\bar{k}_r) > 0$ on the interval $\bar{k}_r \in [0, \bar{k}_{\max}]$. The constraint ensures complete coverage of the wave number line, meaning that each point on the line is covered by at least one satellite pair. Satellite arrangements that violate the lower bound are immediately discarded because they will have gaps in the wave number line, which lead to spatial frequencies that will not be covered.

To solve this problem, an algorithm was implemented that computes the Q function for the fundamental constellation and all its subsets, found by removing one satellite at a time, two at a time, and so forth. Satellite combinations that violate the lower threshold are discarded, and the remaining solutions with a minimum number of satellites, $N_{\min}(m)$, constitute the minimal set. Note that for a given m there may be several different constellations with the same, minimum, number of satellites.

In a fundamental constellation of N_f satellites, there are up to

$$\sum_{k=1}^{N_f}\binom{N_f}{k} = 2^{N_f} - 1 \tag{6}$$

trials that this algorithm may need to make; for large N_f, this is unreasonably large. There are, however, numerous ways to speed up

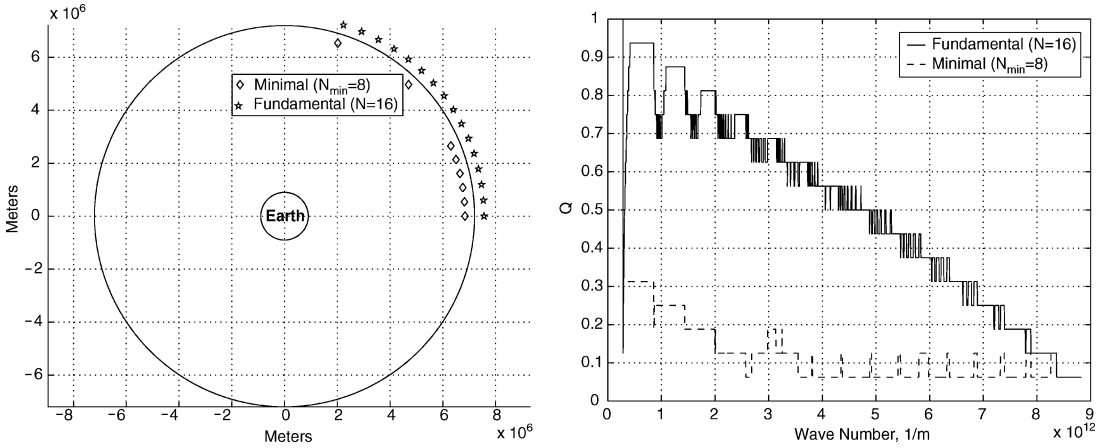

Fig. 2 Fundamental (N_f = 16) and minimal distributions (not to scale), $N_{\min}$ = 8, and Q curves for m = 31.

Table 1 Summary of results for a 7200-km orbit, with $d_{\min}/r_o = 0.0791$

Fundamental number of satellites N_f	Number of pixels $m = 2N_f - 1$	Minimum number of satellites $N_{\min}$	Number of solutions	Lower bound N_{lb}
1	1	1	1	1
2	3	2	1	2
3	5	3	1	3
4	7	4	1	3
5	9	4	2	4
6	11	5	3	4
7	13	5	3	4
8	15	5	1	5
9	17	6	10	5
10	19	6	3	5
11	21	6	2	5
12	23	7	18	6
13	25	7	12	6
14	27	7	4	6
15	29	7	1	6
16	31	8	28	6
17	33	8	19	7
18	35	8	3	7
19	37	9	142	7
20	39	9	91	7

the computation by restricting the space of trials considered, some of which have been used in our computations. This algorithm has been implemented for $m = 3, 5, 7, \ldots, 39$, and the results are summarized in Table 1. Figure 2 shows Q for a fundamental constellation of $N_f = 16$ satellites ($m = 31$ pixels) and a minimum of $N_{\min}(31) = 8$ satellites. The $N_{\min}$ curve shown is the one that maximizes the area under the Q curve over all of the 28 possible constellations with 8 satellites and comprises satellites 0, 1, 2, 3, 4, 5, 10, and 15. Note that the minimal sets may change with the factor $d_{\min}/r_o$ in Eq. (4).

A lower bound on the size of a constellation can be determined as follows. For a constellation of N satellites, there are exactly

$$\binom{N}{2} = \frac{1}{2}N(N-1)$$

baselines. Each baseline provides two pixels, plus one for the self-pixels, which gives a total of $m = N(N-1)+1$. Thus, a lower bound on the number of satellites to cover m pixels is given by

$$N_{\text{lb}} = \text{int}^+\left[\tfrac{1}{2}\left(1+\sqrt{4m-3}\right)\right]$$

where $\text{int}^+[x]$ is the smallest integer larger than or equal to x. A solution can have no fewer than this number of satellites in the constellation without having gaps in the wave number plane. Moreover, there may not exist solutions with $N_{\min} = N_{\text{lb}}$. For example, for $m = 15$, the minimal solution has $N_{\min} = 5$, which is equal to the lower bound. For $m = 29$, the minimal solution has $N_{\min} = 7$, which has one more satellite than the lower bound of 6 (Table 1). For large m, the lower bound is approximately $\text{int}^+[\sqrt{m}]$.

V. Interferometric Observatory

The discussed constellation arrangements will completely cover the wave number plane in half an orbit period, whereas imaging for several orbital periods will result in improved image quality. Thus, over a short period (days at most) an image can be formed. If we place the constellation in an inclined orbit, the orbit plane will precess relative to inertial space and the constellation will scan across the celestial sphere at a constant rate, effectively repeating its coverage after one nodal period. The precession rate of the orbit plane is given by[6]

$$\dot{\bar{\Omega}} = -\left(\tfrac{3}{2}\right)\sqrt{\mu/r_o^3}\left(R_o^2 J_2/r_o^2\right)\cos(\iota)$$

where $R_o = 6378.14$ km is the Earth's radius, $J_2 = 0.00108263$ is the second zonal harmonic of the Earth, $\mu = 3.986005 \times 10^5\ \text{km}^3/\text{s}^2$ is the Earth's gravitational constant, ι is the inclination, r_o is the orbital radius, and $T = 2\pi/\dot{\bar{\Omega}}$ is the precession period of the node. For an 800-km altitude orbit inclined at 45 deg to the equator, the precession period is 77 days. For a constellation in a 45- or 135-deg inclination orbit, every point on the celestial sphere can be imaged with a resolution ranging from θ_r to $\sqrt{2}\theta_r$ within one nodal period. For instance, target objects located at a latitude of ± 45 deg can be imaged once every nodal period with a resolution of θ_r. Objects on the equatorial plane can be imaged twice every nodal period with a resolution ranging from θ_r to $\sqrt{2}\theta_r$. Objects at ± 90 deg can be continuously imaged with a resolution ranging from θ_r to $\sqrt{2}\theta_r$.

An important design consideration is the speed at which the picture frame disk moves in the wave number plane because this affects the image quality. The faster this speed is, the poorer the image quality becomes. Given an upper bound on the wave-plane velocity $\bar{v}$ and a desired angular resolution θ_r, this constrains the angular rate at which the picture frame disk moves in the wave number plane, equal to the mean motion of the orbit, $\omega \le \frac{1}{2}\bar{v}\theta_r$. This bounds the desired orbit radius, $r_o \ge \sqrt[3]{[4\mu/(\bar{v}\theta_r)^2]}$. Thus, the choice of orbit radius does not depend only on the desired baselines (determined from the desired angular resolution), but also on the desired image quality. Note that it is possible to trade a higher speed in the wave number plane (shorter period) with additional observations, to strike a balance between the two.

Other issues of concern are the signal detection, transmission, and interference. Moreover, path length knowledge and/or control down to a fraction of the wavelength is required for a general interferometric observatory. Whereas these issues are in general tractable for long wavelength imaging applications, they will be especially hard for IR missions. Our observatory is well-suited for long wavelength applications. On the other hand, there are certain technologies that are assumed to exist for the proposed very long baseline, Earth-orbiting observatory to be feasible at visible and IR wavelengths, such as heterodyne or a direct detection method.[7–9] Of particular interest is applying a heterodyne detector to IR applications. Such interest is motivated by NASA's ambitious Origins program.[10] Precurser space-based missions of the Origin's program include the Hubble Space Telescope and Stratospheric Observatory for Far Infrared Astronomy, an IR mission. First- (Space Interferometry Mission), second- (Terrestrial Planet Finder[11]), and third- (Planet Imager[12]) generation missions involve the detection of signals with wavelengths ranging from 0.4–0.9 to 20 μm. Heterodyne detection has several advantages over direct detection, has been demonstrated for an IR application[8] and is the subject of ongoing research.

VI. Conclusions

In this Note, we propose a class of sparse aperture interferometric satellite constellations in Earth orbit that can be used to observe astronomical bodies over the full celestial sphere. This observatory is capable of forming high-resolution images in timescales of a few hours, while completely covering the desired region of the wave number (u–v) plane for a wide range of wavelengths. An optimization procedure is defined that supplies m pixels of resolution with a minimum number of satellites. A lower bound for the minimum number of spacecraft in the constellation is derived, and we show that for the example considered this procedure results in an observatory that is within 0–2 satellites from this lower bound. The zonal J_2 effect is used to scan the observatory across the celestial sphere. Finally, we discuss some practical implementation issues for these observatories.

Acknowledgment

This research was supported by NASA Grant NAG 5-10336 with the University of Michigan.

References

[1]Hyland, D. C., "Interferometric Imaging Concepts with Reduced Formation-Keeping Constraints," AIAA Paper 2001-4610, Aug. 2001.

[2]Hyland, D. C., and Al-Twaijry, H., "Formation Control for Optimal Image Reconstruction in Space Imaging Systems," International Symposium on Formation Flying, (submitted).

[3]Hyland, D. C., "The Inverse Huygens-Fresnel Principle and Its Implications for Interferometric Imaging," *Journal of the Astronautical Sciences* (to be published).

[4]Born, M., and Wolf, E., *Principles of Optics*, Pergamon Press, Oxford, 1980, p. 500.

[5]Thompson, A. R., Moran, J. M., and Swenson, G. W., *Interferometry and Synthesis in Radio Astronomy*, Wiley, New York, 1986, Chap. 5.

[6]Roy, A. E., *Orbital Motion*, 3rd ed., Institute of Physics, Philadelphia, 1998, pp. 316–319.

[7]Hale, D. S., Bester, M., Danchi, W. C., Fitelson, W., Hoss, S., Lipman, E. A., Monnier, J. D., Tuthill, P. G., and Townes, C. H., "The Berkeley Infrared Spatial Interferometer: A Heterodyne Stellar Interferometer for the Mid-infrared," *Astrophysical Journal*, Vol. 537, No. 2, 2000, pp. 998–1012.

[8]Townes, H., "Noise and Sensitivity in Interferometry," *Principles of Long Baseline Interferometry*, edited by P. Lawson, Course Notes from 1999 Michelson Summer School, Jet Propulsion Lab., JPL Publ. 00-009, California Inst. of Technology, Pasadena, CA, 2000, Chap. 4.

[9]Kingston, R. H., "Detection of Optical and Infrared Radiation," Springer-Verlag, New York, 1978, Chap. 3, pp. 131–136.

[10]NASA Origins Program, URL: http://origins.jpl.nasa.gov [cited 5 December 2003].

[11]*The Terrestrial Planet Finder: A NASA Origins Program to Search for Habitable Planets*, Jet Propulsion Lab., JPL Publ. 99-003, California Inst. of Technology, Pasadena, CA, 1995.

[12]Planet Quest, URL: http://planetquest.jpl.nasa.gov/index.html [cited 5 December 2003].

New, Fast Numerical Method for Solving Two-Point Boundary-Value Problems

Raymond Holsapple* and Ram Venkataraman†
Texas Tech University, Lubbock, Texas 79409-1042
and
David Doman‡
U.S. Air Force Research Laboratory, Wright–Patterson Air Force Base, Ohio 45433-7531

Introduction

IN physics and engineering one often encounters what is called a two-point boundary-value problem (TPBVP). A number of methods exist for solving these problems including shooting, collocation, and finite difference methods.[1,2] Among the shooting methods, the simple-shooting method (SSM) and the multiple-shooting method (MSM) appear to be the most widely known and used methods.

In this Note a new method is proposed that was designed to include the favorable aspects of the SSM and the MSM. This modified simple-shooting method (MSSM) sheds undesirable aspects of these methods to yield a fast and accurate method for solving TPBVPs. The convergence of the modified simple-shooting method is proved under mild conditions on the TPBVP. A comparison of the MSSM, MSM, collocation (CM) and finite difference methods (FDM) is made for a simple example for which all of these methods converge. Further comparison between the MSM and the MSSM can be found in our earlier work,[3] where we studied an optimal control problem with fixed endpoints for a nonlinear system. For that problem it was shown that the MSM failed to converge while the MSSM converged rapidly.

A general TPBVP can be written in the following form:

$$\dot{y}(t) = f(t, y), \qquad a \le t \le b \tag{1}$$

$$r[y(a), y(b)] = 0 \tag{2}$$

where Eq. (2) describes the boundary conditions satisfied by the system. Examples are the familiar initial-value problem (IVP) and first-order necessary conditions obtained by an application of the Pontryagin Maximum Principle in optimal control theory. TPBVPs from optimal control have separated boundary conditions of the type $r_1[y(a)] = 0$ and $r_2[y(b)] = 0$.

Some of the initial publications that deal with TPBVPs are Keller[4,5] and Roberts and Shipman.[1] Provided it converges, the SSM is the simplest, fastest, and most accurate method to solve TPBVPs. However, it is well known that the SSM can fail to converge for problems whose solutions are very sensitive to initial conditions. For such problems, FDM and CM can provide a solution that satisfies the boundary conditions and is close to the actual solution in some sense. This led to the development of the MSM.[6] Morrison et al.[6] first proposed the MSM as a compromise between the SSM and the finite difference methods. Keller[5] refers to the MSM as parallel shooting and also proposed a version of parallel shooting that he called "stabilized march." The FDM and CM schemes are much

Received 30 April 2003; revision received 15 July 2003; accepted for publication 20 July 2003.

*Graduate Student, Department of Mathematics and Statistics.
†Assistant Professor, Department of Mathematics and Statistics.
‡Aerospace Engineer. Senior Member AIAA.